AIAA 81-4349

Ball-Obturation of a Spinning Tubular Projectile

R.H. Nunn* and J.W. Bloomer II†
Naval Postgraduate School, Monterey, Calif.

Performance improvements in tubular projectiles over conventional rounds are often negated by difficulties in sealing (obturating) the tubular projectiles during their residence in the barrel of the gun. Ball-obturation of a tubular projectile is achieved by the friction-driven gyrodynamic motion of a bored sphere that is mounted loosely within the spinning projectile. In this paper the motion is analyzed by means of solution of the Euler equations of motion, after suitable formulation of the applied moments. A linear form is presented in order to assist in the preliminary design of ball-obturated projectiles and similar systems. The sensitivity of the projectile performance to the various design variables is demonstrated by means of a series of computer experiments.

Nomenclature

A = minor moment of inertia of ball (about hole axis)
C = major moment of inertia of ball
D = step input for linear approximation
h = thickness of gap between ball and projectile
k = ratio of gas specific heats (1.4 for air)
M = applied torque
M_∞ = launch Mach number
P_∞ = launch level pressure
r_p = radius of hole in projectile
r_s = radius of hole in ball
R = slope of ramp for linear approximation
R_s = radius of ball
t = time
ζ = damping ratio for linear approximation
θ,ϕ,ψ = Euler angles
λ = $C/A-1$
μ = molecular viscosity of fluid in gap
μ_s = coefficient of sliding friction
ρ_s = density of ball material
ω = angular velocity
ω_{po} = projectile initial rate of spin

Subscripts

o = torque-free solution
r = relative angular velocity
x,y,z = components relative to the coordinate axes

Superscripts

$(\bar{\ })$ = dimensional quantity (absence of overbar above a time-dependent quantity indicates that it has been nondimensionalized through the use of ω_{po})
$(*)$ = conditions at initial opening of path along projectile axis

Introduction

THE tubular projectile is not a new concept. As early as 1858, the usefulness of tubular projectiles was recognized for specific applications. In that year, Joseph Whitworth wrote about and illustrated a tubular projectile that was hexagonal in cross section, with a circular hole, and utilizing a wooden sabot.[1] Whitworth noted its particular ". . . effectiveness in perforating elastic materials which prevented them from closing up," and further claimed that the tubular projectile penetrated deeper into masonry than any other with which he was acquainted. According to Charters and Thomas,[2] the Krnka-Hebler Projectile was reported in *Allgemeine Schweitzerische Militarzeitung* as having been so successful that the U.S. Ordnance Department carried out firing tests of caliber 0.30 projectiles in 1894. In these tests, a vulcanized fiber sabot was used to push the projectile out of the barrel. More sophisticated tests, conducted some 50 years later,[2] essentially confirmed the improvements in projectile drag reported in 1894. Further developments in the history of the tubular projectile and description of its general benefits and drawbacks are presented in Ref. 3.

A central problem associated with projectiles that do not completely block (obturate) the gun breech and barrel is the sealing of the propulsion gases in order to obtain and maintain the required high chamber pressures. In the tubular projectile the hole in the projectile which allows shock-swallowing (and attendant reduction in drag) during flight also allows pressure venting (and misfire) during launch. A number of tubular projectile designs include obturation schemes that simply plug the projectile during launch (as in Whitworth's design) with the plug falling away as the projectile leaves the barrel. These plugs, however, can become the FOs in FOD (foreign object damage) and are unacceptable as obturators in many applications, particularly in aircraft guns.

A recent design innovation[4] consists of a two-part tubular projectile in which a bored sphere is loosely mounted within a spherical cavity contained in an otherwise standard tubular projectile. The photograph in Fig. 1 illustrates the general configuration. During launch the ball is held in a blocking position by the high-pressure propulsion gases. The projectile and ball move together down the barrel and attain the same high forward and rotational speeds. When the ball/projectile system leaves the barrel, the propulsion pressure is relieved and the net pressure force on the ball is reversed in direction and greatly reduced in magnitude. In a properly designed system the ball is then free to move within the projectile and, with the passage of time, will orient itself such that the two holes are aligned and the tubular passage is opened. Obturation is thereby achieved during launch with automatic opening of the tubular passage following launch and during free flight.

The goal of the investigation reported herein has been to fully understand the motion of the ball within the projectile and to thereby gain the capability of defining a "properly designed" system. The motion may be characterized as friction-driven and gyrodynamic in nature. Although the solution method is applicable to a variety of similar problems, in this paper the analysis is described as it applies to the ball-obturated projectile (BOP) system. A linear form is developed to aid in preliminary design work and the results of a series of computer experiments are reported in order to indicate the sensitivity of the BOP performance to the various design variables.

Received Oct. 14, 1980; revision received March 9, 1981. This paper is declared a work of the U.S. Government and therefore is in the public domain.

*Associate Professor of Mechanical Engineering. Associate Fellow AIAA.
†Lieutenant, U.S. Navy.

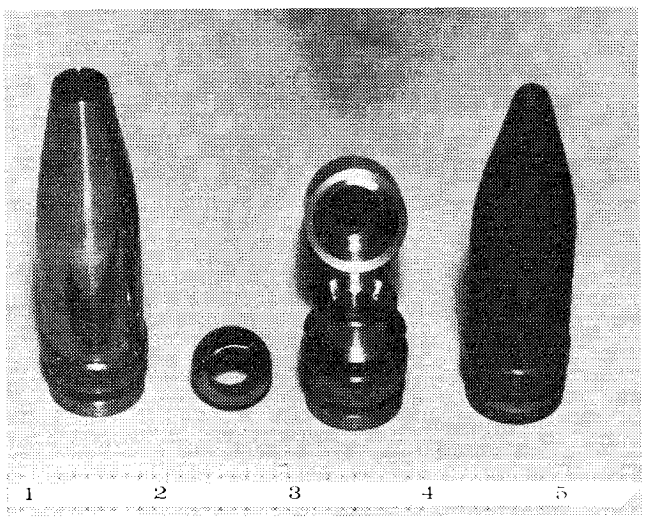

Fig. 1 Photograph of ball-obturated projectile and standard projectile; 20 mm. (Courtesy of Naval Weapons Center, China Lake, Calif.)

Analysis

Figure 2 illustrates the coordinate systems employed in the analysis. The X, Y, Z axes are fixed in space and the axis of projectile spin is taken to be the Z axis. The x, y, z axes are fixed to the ball with the z axis aligned with the hole. The orientation of the ball axes with respect to the fixed axes is defined by the Euler angles ψ, ϕ, and θ. The rates of ball precession and spin are $\dot{\psi}$ and $\dot{\phi}$, respectively, and θ is the angle of tilt of the ball hole axis measured from the projectile spin axis.

The torque applied to the ball as it rotates within the spinning projectile is due to the relative motion between the two bodies. The applied torque vector is therefore oriented in a direction opposite to the vector of relative angular velocity. When this fact is incorporated into the governing equations of motion (Euler's equations for principal axes) and they are written in terms of the Euler angles, they may be presented in the following form[3]:

$$\ddot{\psi} = -M(\dot{\psi}-1) + \dot{\theta}[(\lambda+1)\dot{\phi} + (\lambda-1)\dot{\psi}\cos\theta]/\sin\theta \quad (1a)$$

$$\ddot{\phi} = -[M/(\lambda+1)][(\dot{\psi}-1)\cos\theta + \dot{\phi}] + \dot{\psi}\dot{\theta}\sin\theta - \ddot{\psi}\cos\theta \quad (1b)$$

$$\ddot{\theta} = -M\dot{\theta} - \dot{\psi}\sin\theta[(\lambda-1)\dot{\phi} + \lambda\dot{\psi}\cos\theta] \quad (1c)$$

where $M = \bar{M}/A\omega_{po}^2\omega_r$.‡ The term $\lambda = (C/A) - 1$ reflects the inertial imbalance of the ball and $\bar{M}$ is the magnitude of the applied torque vector. In the case of gravity-dominated motion, experiments have shown[3] that the torque may be adequately predicted by accounting for fluid shear and sliding friction. The same result can be expected in the case of the ball obturator under aerodynamic loads but the expression for the effect of sliding friction is somewhat more complex than for the gravity-dominated situation.

Applied Torques

The magnitude of the total applied torque due to fluid shear is given by

$$\bar{M}_f = 8\pi(1+\epsilon)\mu R_s^3\bar{\omega}_r/3\epsilon \quad (2)$$

This expression arises from the assumption of laminar Couette flow in the gap between the ball and the projectile with thickness $h = \epsilon R_s \ll R_s$. (The relative angular velocities between the two bodies are insufficient to stimulate turbulent flow in the gap under representative conditions.)

‡Time-dependent quantities are nondimensionalized through the use of ω_{po}. Dimensional forms of these quantities are indicated by the overbar.

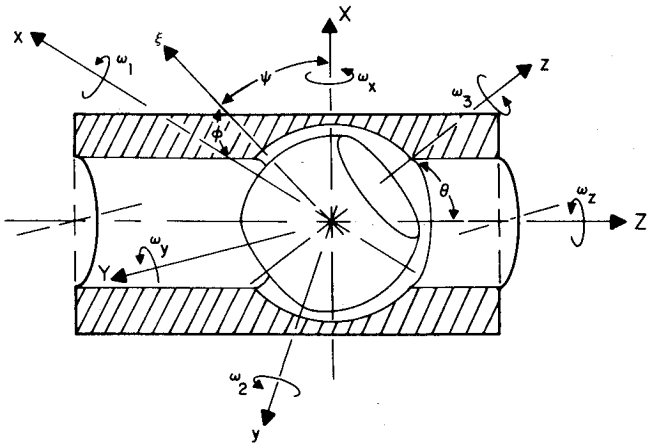

Fig. 2 Sketch showing angles, angular velocities, and coordinates used in the analysis.

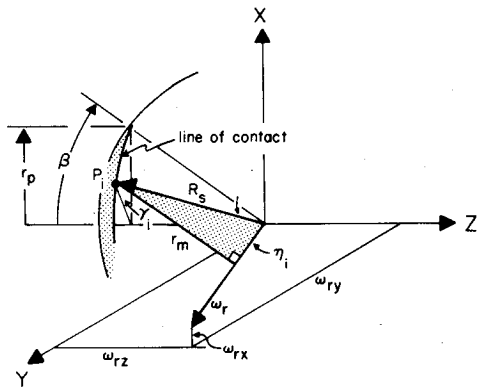

Fig. 3 Sketch illustrating the line of contact between ball and projectile.

In the case of sliding friction it is assumed that aerodynamic forces on the ball cause it to contact the projectile along the line defined by the hole in the projectile intersecting with the surface of the ball. Figure 3 illustrates the geometry of the problem. The exact expression of the aerodynamic forces is indeed a complex problem. With the ball blocking the hole in the projectile the hydrodynamic obstruction to the oncoming supersonic flow will resemble a blocked tubular cylinder with cavities at both upstream and downstream ends. At the upstream end a curved detached shock will exist with normal-shock effects over a portion of the blunt nose. Upstream face pressures will range between the stagnation pressure downstream of a normal shock and a pressure that is reduced due to flow spillage around the rim of the projectile. Further reductions in pressure below stagnation pressure can be expected because of the complex recirculating shear flow within the cavity ahead of the ball.

Base pressures on projectile shapes are generally less than freestream ambient pressure and in the Mach number range of interest here ($3 < M_\infty < 5$) they are likely to be on the order of $0.5P_\infty$.[5] For our purposes we wish to estimate an aerodynamic force that is on the low side of the range of uncertainty since this will lead to conservative predictions (on the high side) for the elapsed times of ball opening. At the Mach numbers of interest the upstream stagnation and static pressures behind a normal shock are not greatly different (about 10% variation) and the selection of static pressure as the effective pressure on the face of the ball will lead to approximate predictions on the conservative side. A conservative estimate for the base pressure is P_∞. In any case, since the body is very blunt with the hole blocked, the base pressure

will have relatively little effect upon the aerodynamic force on the ball. The pressure differential across the ball is therefore taken to be the static pressure downstream of a normal shock at M_∞, less the freestream static pressure. The resulting expression for the aerodynamic force on the ball is:

$$F_a = \pi r_p^2 P_\infty [2k(M_\infty^2 - 1)/(k+1)] \tag{3}$$

For a typical 20-mm projectile configuration at $M_\infty = 3.5$, sea-level, this force will be on the order of 100 N. When the ball is in a partially open orientation the magnitude of the pressure force will decrease (ultimately vanishing when the holes are aligned) and a moment will arise due to the flow through the skewed hole. In this situation the simple expression given by Eq. (3) will be inappropriate and a more sophisticated analysis will be required. Subsequent results stem from the use of Eq. (3) and are therefore not valid for ball orientations in which substantial through-flow occurs.

Along the line of contact between the ball and the projectile the aerodynamic force, F_a, will be balanced by a reaction force given by F_a/n where n is the number of contact points. The sliding friction force at each point of contact will then be $(F_a/n)\mu_s \cos\beta$ and the moment due to these forces is:

$$\bar{M}_{sa} = \mu_s F_a \cos\beta \left[\sum_{i=1}^{n} (r_m)_i\right] \Big/ n \tag{4}$$

where $(r_m)_i$ is the moment arm extending from the ith contact point and directed normal to the vector of relative angular velocity. From the geometry of the problem (Fig. 3) the magnitudes of these moment arms are given by:

$$(r_m)_i = R_s \sin\eta_i$$

and the angle η_i is given by:

$$\eta_i = \cos^{-1}(\boldsymbol{P}_i \cdot \boldsymbol{\omega}_r / R_s \omega_r)$$

With unit vectors $\boldsymbol{e}_x$, $\boldsymbol{e}_y$, and $\boldsymbol{e}_z$ for the fixed coordinate system,

$$\boldsymbol{P}_i = R_s(\boldsymbol{e}_x \sin\beta\cos\gamma_i + \boldsymbol{e}_y \sin\beta\sin\gamma_i + \boldsymbol{e}_z\cos\beta)$$

and

$$\boldsymbol{\omega}_r = \boldsymbol{e}_x\omega_{rx} + \boldsymbol{e}_y\omega_{ry} + \boldsymbol{e}_z\omega_{rz}$$

we have

$$(r_m)_i/R_s = \{1 - [(\omega_{rx}/\omega_r)\sin\beta\cos\gamma_i + (\omega_{ry}/\omega_r)\sin\beta\sin\gamma_i + (\omega_{rz}/\omega_r)\cos\beta]^2\}^{1/2}$$

For a given geometry, $\beta[=\sin^{-1}(r_p/R_s)]$ is fixed and the γ_i locate each contact point on the line of contact. The components (ω_{rx}, ω_{ry}, and ω_{rz}) of the relative angular velocity vector are calculable from the Euler angles and their rates at each instant in time.

The exact number and location of the contact points is difficult to predict and may depend upon individual BOP designs. However, any effect of an arbitrariness in contact point specification is "blurred" by the high-speed rotary motion and errors resulting should be random and therefore of little influence on the overall motion. This hypothesis has been verified by computer experiments in which as many as ten contact points were found to give results that were essentially the same as for the first stable configuration consisting of three contact points. This latter situation has been chosen as being representative of the general case. That is, $n=3$ and $\gamma_i = \gamma_{i-1} + 2\pi/3$.

Equations (2-5) allow the evaluation of the torque terms in Eq. (1) and the system of equations may be integrated according to the appropriate initial conditions. These are:

$$\psi(0)=0 \qquad \theta(0)=\theta_o \qquad \phi(0)=0$$

$$\dot{\psi}(0)=1 \qquad \dot{\theta}(0)=0 \qquad \dot{\phi}(0)=0$$

Computer solution has been achieved by means of a fourth-order Runge-Kutta routine employing a variable step-size to control numerical errors. Figure 4 illustrates the nature of the ball motion for several projectile spin rates and Fig. 5 shows the variations of nutation, precession, and spin rates for a typical case. In these figures, the parameters are those of the "baseline" projectile configuration described in Table 1.

Two system constraints have been investigated in the analysis. In the first case we have invoked the constraint of constant projectile spin rate and, in the second case, we have required a constant system (ball plus projectile) kinetic energy.

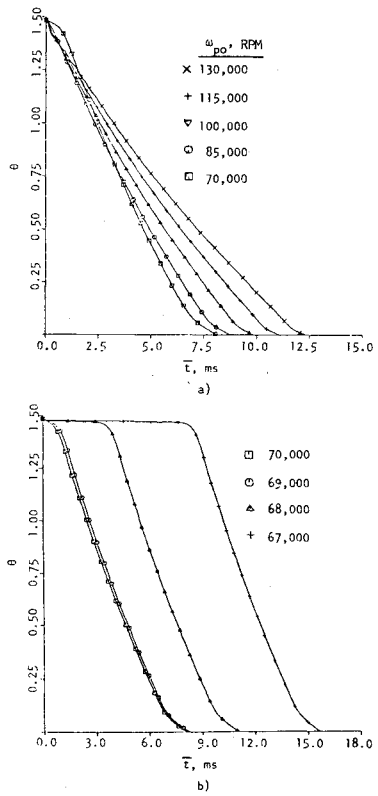

Fig. 4 Exact solutions for θ vs $\bar{t}$; baseline projectile. a) High projectile spin rates; b) low projectile spin rates.

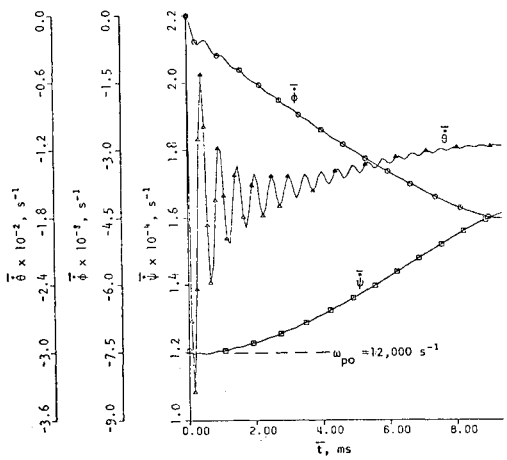

Fig. 5 Euler angle rates for a typical case; baseline projectile, $\omega_{po} = 1.20 \times 10^4$ s^{-1} (115,000 rpm).

Table 1 Ranges of design variables

Design variable	Minimum	Baseline	Maximum	Fig. No.
R_s, mm	Baseline	7.90	39.5	8
A, Nms^2		2.24×10^{-7}	7.00×10^{-4}	
r_s/R_s	0.400	0.598	0.800	9
A, Nms^2	3.20×10^{-7}	2.24×10^{-7}	1.00×10^{-7}	
λ	0.19	0.41	0.69	
ρ_s, kg/m^3	3.10×10^{3}	7.75×10^{3}	1.24×10^{4}	10
A, Nms^2	8.96×10^{-8}	2.24×10^{-7}	3.58×10^{-7}	
μ_s	0.71	0.855	1.000	11
M_∞	3.00	3.50	5.00	12
P_∞, atm	0.1	1.0	Baseline	13
ω_{po}, s^{-1}	6.91×10^{3}	1.20×10^{4}	1.36×10^{4}	4,7
θ_o, deg	70	85	Baseline	6

Since the inertia of the ball is small relative to that of the projectile (a factor of about 20 in the baseline case) the decrease in projectile spin rate necessary to maintain constant system kinetic energy during the ball motion is rather small (typically about 2%) and the two cases are not significantly different. The computer solutions shown here (so-called "exact" solutions) are for the case of constant system kinetic energy.

Linearized Analysis

From Figs. 4a and 4b it will be noted that there is a marked change in the nature of the ball motion at a projectile spin rate of about 7300 s^{-1} (70,000 rpm). At rates above this value (Fig. 4a) the ball motion appears to be quite linear; that is, the response of the ball to the frictional torques approximates one of a second-order linear system responding to a combined ramp and step input (both of which are negative). Such a response is given by

$$\theta=\theta_o+D+R(t-2\zeta)+\exp(-\zeta t)\{R\sin[(1-\zeta^2)^{1/2}t+\Phi_R]$$
$$-D\sin[(1-\zeta^2)^{1/2}t+\Phi_D]\}/(1-\zeta^2)^{1/2} \quad (6)$$

where

$$\Phi_R/2=\Phi_D=\tan^{-1}[(1-\zeta^2)^{1/2}/\zeta]$$

The parameters of the response are derived elsewhere[3] and are given by:

$$\zeta=M/2 \qquad D=-(\lambda/2)\sin2\theta_o \qquad R=MD/(\lambda+1)$$

The method leading to the linear approximation is a perturbation upon the equilibrium solution to Eq. (1) under torque-free conditions. As shown in Ref. 6, this solution (designated by subscript o) is given by $\dot\theta_o=0$, $\dot\psi_o=1$, and $\dot\phi_o=-\lambda\cos\theta_o/(\lambda+1)$, and the perturbation results in the constraints that $M\ll1$ and $R\ll1$. Under these conditions the relative angular velocity is approximated by

$$\omega_r\simeq\lambda\cos\theta_o/(\lambda+1)$$

and the normalized torque is given by

$$M=\bar M/(A\omega_{po}^2\omega_r)=(\lambda+1)\mu_sF_a\iota\cos\beta/(\lambda nA\omega_{po}^2\cos\theta_o) \quad (7)$$

where

$$\iota=\sum_{i=1}^{n}(r_m)_i$$

The fluid shear term is omitted in this expression since, in the application at hand, it is negligible in comparison with the torque due to sliding friction (about five orders of magnitude smaller).

The moment arm term, given by Eq. (5), must also be linearized and to accomplish this it is necessary to construct a suitable mean value that is valid over the range of ball motion. Linearization of the equations relating the components of angular velocity to the orientation of the ball (the Euler angles) leads to the following approximate expressions:

$$\omega_{rx}/\omega_r\simeq\sin\theta_o\sin\psi_o \qquad \omega_{rz}/\omega_r\simeq\cos\theta_o$$
$$\omega_{ry}/\omega_r=[1-(\omega_{rx}/\omega_r)^2-(\omega_{rz}/\omega_r)^2]^{1/2}\simeq\sin\theta_o\cos\psi_o$$

Since the linearization requires that $\sin2\theta_o\ll1$ we are constrained to initial ball tilt angles near 90 deg so that $\cos\theta_o\ll1$ and

$$\omega_{rx}/\omega_r\simeq\sin\psi_o \qquad \omega_{rz}/\omega_r\simeq0 \qquad \omega_{ry}/\omega_r\simeq\cos\psi_o$$

which is to say that in the linear approximation, valid for small torques, the relative angular velocity vector will not deviate significantly from the plane normal to the projectile spin axis. The relative motion in such cases is mainly due to the nutation rate ($\dot\theta$) with the sum of the spin and precession rates remaining approximately equal to the projectile spin rate.

With these approximations the expression for the ith moment arm may be written

$$(r_m)_i=R_s[1-\sin^2\beta\sin^2(\psi_o+\gamma_i)]^{1/2}$$

A mean value of this expression over one cycle of rotation of ψ_o (the other terms being constants) is sought. With $\alpha=\psi_o+\gamma_i$ this mean may be expressed as

$$[(r_m)_i/R_s]_{\text{mean}}=1/2\pi\int_0^{\pi/2}(1-\sin^2\beta\sin^2\alpha)^{1/2}\,d\alpha$$

which may be written

$$[(r_m)_i/R_s]_{\text{mean}}=2/\pi E(\beta)$$

where $E(k)$ is the complete elliptic integral of the second kind.[7] Note that this mean is independent of the location of the contact points so that for n contact points

$$\iota/R_s=2n/\pi E(\beta)$$

and the linearized expression for the normalized moment becomes

$$M=2(\lambda+1)\mu_sF_aR_sE(\beta)\cos\beta/(\pi\lambda A\omega_{po}^2\cos\theta_o) \quad (8)$$

which is, again, independent of the number and location of contact points. With M thus approximated the damping ratio ζ and decay rate R are known and the approximate response may be calculated from Eq. (6).

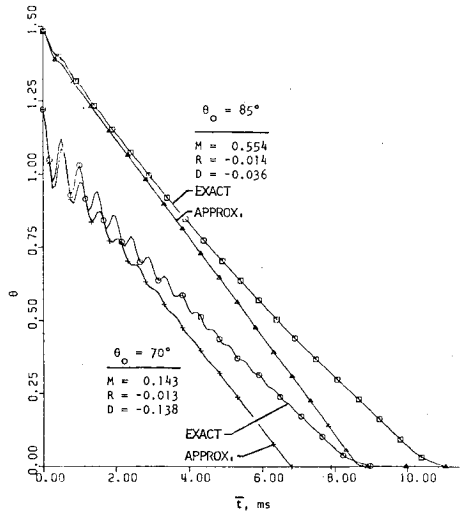

Fig. 6 Comparison of approximate solutions with exact solutions; baseline projectile, $\omega_{po} = 1.20 \times 10^4$ s^{-1}.

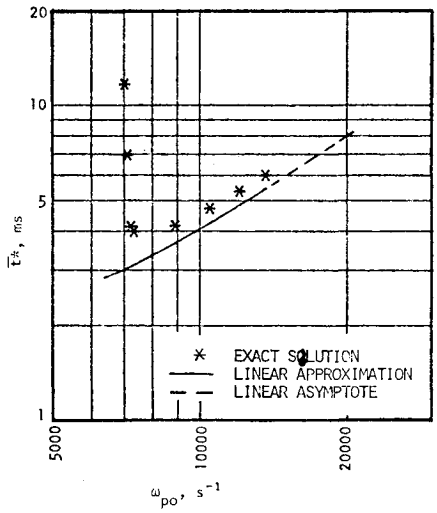

Fig. 7 Comparison of approximate solutions with exact solutions. Effect of projectile spin rate on initial opening time.

Figure 6 shows a comparison of the linear approximation with the exact solution for the motion of the baseline model at the nominal spin rate of 115,000 rpm. Two initial ball tilt angles are also shown and it may be seen that the linear approximation yields results that are quite acceptable for initial angles near 90 deg. The values of M,R, and D are given on the figure for reference purposes. The usefulness and limitations of the approximate method are also illustrated in Fig. 7 where the initial opening time is given as a function of projectile spin rate. This time, designated as t^*, is the time required for a straight-through path to open along the projectile centerline. The ball tilt angle at this instant is given by

$$\theta^* = \sin^{-1}(r_s/R_s)$$

and the corresponding time is a useful reference quantity for comparison of various obturator designs. (In addition, the aerodynamic force model used in this analysis becomes highly suspect at values of θ below θ^* since the simple shock structure assumed here will be invalid if there is any significant flow through the projectile.)

Figure 7 indicates that the linear approximation approaches the exact solution at large values of ω_{po}. This is to be expected since M decreases quadratically with ω_{po}. The asymptotic behavior of $\bar{t}^*$ at high ω_{po} is a useful design insight and is given by

$$\bar{t}^*_\infty = A\omega_{po}[(\theta_o - \theta^*) + D]/\bar{M}\sin\theta_o$$

and for the baseline case this reduces to $\bar{t}^*_\infty \simeq 4.0 \times 10^{-4}$ ω_{po}ms(ω_{po} in s^{-1}). The sharp minimum in $\bar{t}^*$ illustrated in Fig. 7 suggests some caution in the design of these devices and also provides encouragement regarding the existence of criteria leading to an optimum design. The low spin-rate behavior shown in Fig. 7 is outside the linear range of operation and is due to the delaying mechanism of sliding friction at relatively large values of M (large friction, low inertial imbalance due to a small hole in the ball, and/or low projectile spin rate). Under these conditions the ball "hovers" at its initial value and considerable time elaspses before a ball orientation is achieved in which friction is in a direction to aid the alignment of the hole with the projectile axis. This behavior is also illustrated in Fig. 4b, and such conditions are obviously to be avoided in the system design.

Sensitivity Analysis

The design variables affecting the obturator performance are those contained in the normalized torque determined by Eqs. (2-5). The influence of the time-varying relative angular velocity and moment arms in these expressions may be qualitatively evaluated by referring to the linear approximation so that the relevant design variables are [Eq. (8)] λ, μ_s, F_a, β, θ_o, R_s, and ω_{po}. Since λ and β are geometric parameters depending upon the radii of the ball and its hole, and the minor moment of inertia, A, depends upon these as well as the density of the ball material, this list may also be written: r_s, R_s, ρ_s, μ_s, M_∞, P_∞, and ω_{po}. Here the aerodynamic force has been replaced by means of Eq. (3) and the projectile hole is assumed to be of the same size as that of the ball ($r_p = r_s$). In considering the coefficient μ_s, it must be remembered that it depends upon the two materials (ball and projectile) and is therefore dependent upon ρ_s. The independent variation in μ_s has been studied, however, since its value is subject to considerable uncertainty. Experiments have shown[3] that the value of μ_s should be approximately 50% larger than that published for dry friction between smooth surfaces. Table 1 indicates the baseline value for these design variables as well as the maxima and minima that determine the range of the sensitivity analysis. In each case (except ω_{po}, which has been previously discussed) the values of the variables were chosen such that equal increments were provided and the baseline condition was included in the range. Single parameter variations are shown here although work is continuing using the techniques of numerical optimization.

The computer data are presented as θ vs $\bar{t}$ and the interested reader may construct cross plots such as that of Fig. 7 to evaluate the effects of these design variables upon the time required to reach a given angle, such as θ^*. Figures 8-13 illustrate the relative importance of the selected design variables. It is important to note that in these figures the range of system performance has been restricted to the quasilinear range previously discussed where the ball response is typically of the type shown in Fig. 4a and above the minimum in Fig. 7. Outside of this range (in the "hovering" state) the trends illustrated may be reversed. Attempts to reduce ball response time by the design improvements suggested by Figs. 8-13 may push the performance beyond the minimum illustrated in Fig. 7, with resulting "negative improvements." In many cases the implications of Figs. 8-13 are self-evident but to assist in physical interpretation a few explanatory remarks are offered below.

Geometry Effects

Both the ball radius, R_s, and the radius of the ball hole, r_s, were varied independently. Figure 8 shows the effects of increasing the ball radius while maintaining a constant value

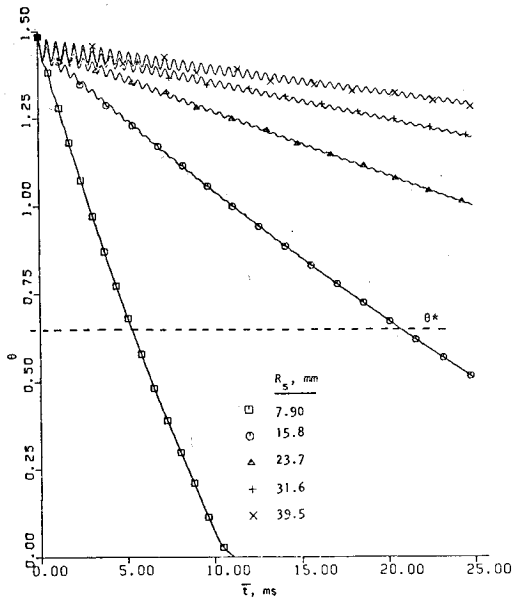

Fig. 8 Effect of ball size on ball response.

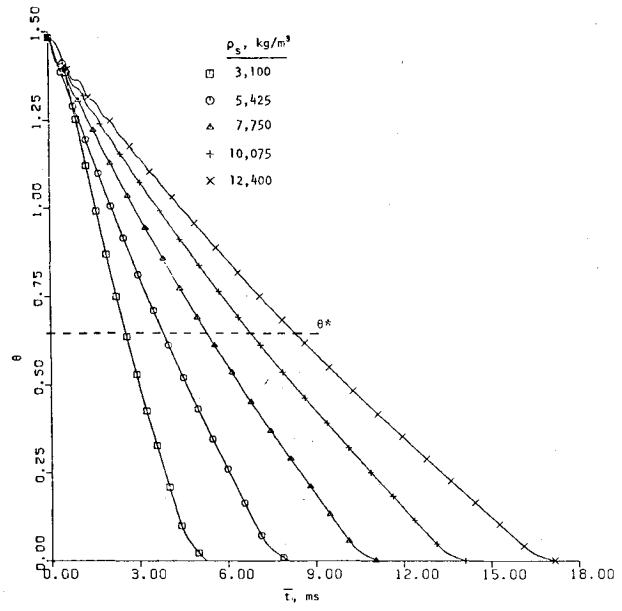

Fig. 10 Effect of density of ball material on ball response.

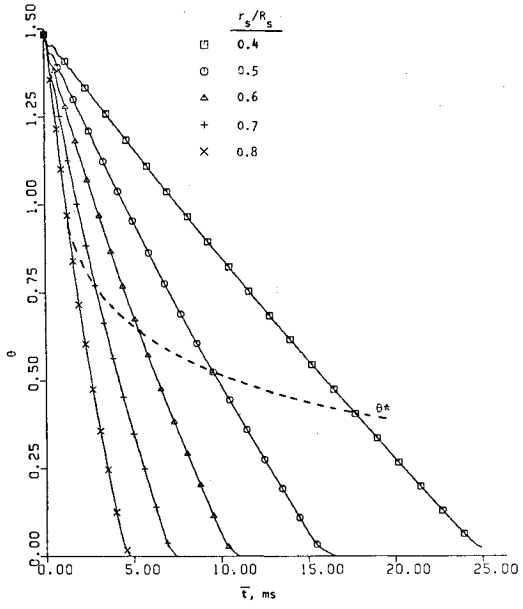

Fig. 9 Effect of ball hole size on ball response.

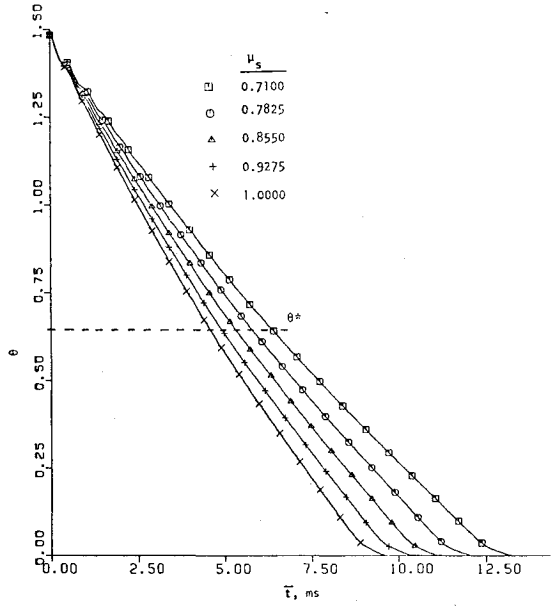

Fig. 11 Effect of coefficient of sliding friction on ball response.

of r_s/R_s. The variation in this case is essentially one of scale-up which covers a range of projectile diameters from, roughly, 20 to 100 mm. It may be seen that larger systems respond more slowly. Increases in applied torques are not sufficient to offset the effects of the fifth-power relationship between ball inertia and radius. Figure 8 indicates that opening of the ball obturator in large projectiles may be unacceptably slow unless compensating design actions are taken. As will be seen in subsequent figures, such actions might include increases in ball hole radius and reduction in the density of the ball material.

Increasing the size of the hole in the ball, with all other parameters held constant, reduces the inertia of the ball and increases the imbalance between the moments of inertia about the two principal axes. Both effects are conducive to rapid ball response and this is illustrated in Fig. 9. In addition, the initial opening angle, θ^*, is directly increased by an increase in r_s/R_s with a corresponding decrease in the elapsed time.

Material Effects

Though the ball-obturator must be of sufficient strength to plug the projectile during launch, it does not contribute to the structural integrity of the projectile in flight. The ball material may therefore be open to some design variation and this possibility is investigated in Fig. 10 where it is seen that the time required to reach a given ball angle is approximately proportional to the density of the ball material, ρ_s. A change in ball material from carbon steel ($\rho_s \sim 7750$ kg/m^3) to an aluminum alloy ($\rho_s \sim 3100$ kg/m^3) would lead to a halving of the response time. This effect also leads to an opportunity of linearly tailoring the ball response time by means of its density—a feature that may be particularly useful in applications of the system as a hydromechanical switch.

Coefficient of Sliding Friction

As has been mentioned, the correct value of μ_s is subject to considerable uncertainty. Figure 11 shows the impact of an

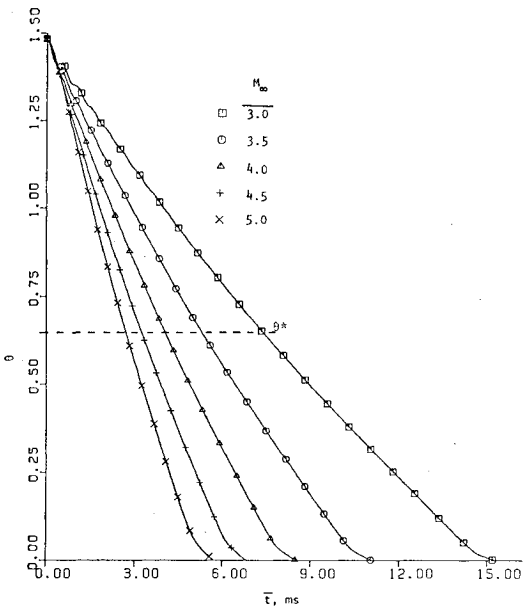

Fig. 12 Effect of launch Mach number on ball response.

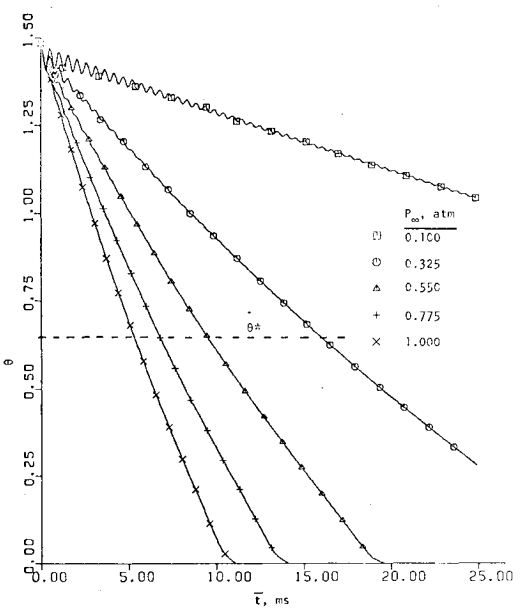

Fig. 13 Effect of launch level pressure on ball response.

uncertainty range of about ±20% in μ_s which, in terms of $\bar{t}^*$, is about ±15%. In applications for which margins of error such as this are unacceptable, tests of prototype configurations may be necessary to determine μ_s. The range tested in Fig. 11 represents our best estimate for dry friction of steel on steel for the range of r_s/R_s covered in Fig. 9. Systems using dissimilar materials will require appropriate changes in μ_s. In addition, it may be seen that some roughening of the interfacial surfaces may not be detrimental to the system performance while intentional polishing of the surface may lead to slower ball action.

Launch Conditions

Projectile launch Mach number and altitude have been separately investigated with the results shown in Figs. 12 and 13. The increases in wave drag associated with higher Mach numbers are actually beneficial in terms of ball response, because of the corresponding increases in the applied torques that aid the motion of the ball within the projectile. On the other hand, increases in launch altitude lead to increases in ball response time. In proceeding from sea-level to a flight-level pressure of 0.325 atm (about 30,000 ft in the standard atmosphere), for example, a threefold increase in $\bar{t}^*$ is predicted for the baseline design.

Conclusion

When a spherical ball with a hole in it is spun within another body, such as a spinning tubular projectile, the orientation of the ball will change so that the hole axis (axis of major moment of inertia) is aligned with the axis of spin. This behavior has been exploited for the purpose of providing automatic opening of a ball-obturator within a spinning tubular projectile. In the case of a typical 20-mm design the opening time is on the order of 10 ms.

An analytical model has been developed in which the torques applied to the ball arise from the relative motion of the two bodies together with the aerodynamic forces acting on the ball. Postulation of a simple form for these forces has led to mathematical expressions for the applied torques and subsequent solution of the Euler equations governing the motion of the ball. Over a wide range of conditions the motion is quasilinear and an approximate solution has been developed and shown to be valid in this range. In the nonlinear range the ball will "hover" about its initial condition and the time required for the alignment is greatly increased.

Ranges of feasible designs have been identified and the influence of several design variables has been evaluated. In general, for rapid ball alignment a ball of a given size should be light in weight and have a large hole. Ball alignment is accelerated at high launch Mach numbers and low launch altitudes. These observations must be tempered with an awareness of a reversal in trends when a design is such that hovering occurs—there is a minimum achievable time for ball alignment.

Although the analysis is adequate for preliminary design purposes there are several areas of investigation that would lead to improvements. A more sophisticated model for the aerodynamic loads is needed, particularly at ball orientations in which flow is possible through the projectile. Research is needed regarding the coefficient of sliding friction for such geometries, especially with regard to the intermittent surface contact during the ball motion. Other applications, such as hydromechanical switching, may require an evaluation of the system for fluids other than air (in which case higher gap Reynolds numbers may lead to an important role for fluid shear between the two bodies).

Acknowledgment

The work described in this paper has been supported, in part, by Code 32052 of the Naval Weapons Center, China Lake, Calif.

References

[1] Whitworth, J., *Miscellaneous Papers on Mechanical Subjects,* J. and J. Thomsons, London, 1858.

[2] Charters, A.C. and Thomas, R.H., "Retardation of Tubular Projectiles Developed from 20 mm American Ball," Ballistics Research Laboratory, Aberdeen Proving Grounds, Report 460, April 1944.

[3] Bloomer, J.W. II, "Ball Obturation of a Spin Stabilized Tubular Projectile," Mechanical Engineer Thesis, Naval Postgraduate School, Monterey, Calif., June 1980 (NTIS No. A092410).

[4] Black, W., "Ball Actuated Tubular Projectile," patent disclosure, Navy Case No. 63902, 1978.

[5] Chang, P.K., *Separation of Flow,* Pergamon Press, New York, 1970, pp. 541-553.

[6] Thomson, W.T., *Introduction to Space Dynamics,* Wiley, New York 1961, pp. 117-118.

[7] Abramowitz, M. and Stegun, I.A., (eds.), *Handbook of Mathematical Functions,* National Bureau of Standards, Washington, D.C., 1964, pp. 589-618.